Lung Perfusion CT:
The Differentiation of Cavitary Mass

Young Han Lee

The Graduate School

Yonsei University

Department of Medicine

Lung Perfusion CT:
The Differentiation of Cavitary Mass

Directed by Professor Myung Soon Kim

The Doctoral Dissertation
submitted to the Department of Medicine,
the Graduate School of Yonsei University
in partial fulfillment of the requirements
for the degree of Doctor of Philosophy

Young Han Lee

June 2007

This certifies that the Doctorial Dissertation
of Young Han Lee is approved.

_____

Thesis Supervisor: Professor Myung Soon Kim

_____

Professor Ki Joon Sung : Thesis Committee Member

_____

Professor Soon-Hee Jung : Thesis Committee Member

_____

Professor Suk Joong Yong : Thesis Committee Member

_____

Assistant Professor Woocheol Kwon : Thesis Committee Member

The Graduate School
Yonsei University
June 2007

Acknowlegdment

First of all, I appreciate my dissertation advisor, professor Myung Soon Kim for introducing me to radiology and supporting me in my pursuit of this field.

I appreciate my dissertation committees, professor Ki Joon Sung, professor Soon-Hee Jung, professor Suk Joong Yong, and professor Woocheol Kwon for providing me with the much needed advice. Especially, I appreciate professor Woocheol Kwon for introducing me to this world of the lung perfusion CT and providing me much advice and discussion.

Thanks to all the radiology professors for making my graduate school a great experience and their advice. Their advices help my completion of this dissertation. I also thank my colleagues in department of radiology for help in reviewing and editing the manuscript for English style and structure.

I would like to deeply thank my family for their endless love, support, and encouragement. I would like to share the joy of completing this dissertation with my lovely wife Joo Hee.

Finally, I thank the Lord. This dissertation and the effort of its pursuit are dedicated to Him.

June 2007

Written by author

Contents

List of Figures ····· ii

List of Tables ····· iii

Abbreviations ····· iv

Abstract ····· v

I. Introduction ····· 1

II. Materials and Methods ····· 3

2.1. Patients selection ····· 3

2.2. Methods ····· 3

2.2.1. Dynamic CT imaging studies ····· 3

2.2.2. Lung perfusion maps ····· 4

2.2.3. Image Analysis ····· 5

2.2.4. Statistical Analysis ····· 6

III. Results ····· 8

3.1. Lung CT perfusion features ····· 8

3.2. Interobserver agreement ····· 8

3.3. ROC Analysis ····· 9

IV. Discussion ····· 18

V. Conclusion ····· 23

References ····· 24

Abstract in Korean ····· 29

List of Figures

Figure 1. Perfusion source images ····· 11

Figure 2. Graphs of the ROC curves for cavitary masses ····· 12

Figure 3. Chest CT and parametric perfusion maps in a 55-year-old man with a lung abscess in the right lower lobe superior segment ····· 13

Figure 4. Chest CT and parametric perfusion maps in a 63-year-old woman with tuberculosis in the left upper lobe apicoposterior segment ····· 14

Figure 5. Chest CT and parametric perfusion maps in a 35-year-old man with squamous cell carcinoma in the left upper lobe apicoposterior segment.····· 15

Figure 6. Chest CT and parametric perfusion maps in a 55-year-old man with squamous cell carcinoma in the right upper lobe·· 16

Figure 7. Chest CT and parametric perfusion maps in a 71-year-old woman with adenocarcinoma in the right middle lobe. ····· 17

List of Tables

Table 1. CT perfusion characteristics of Cavitary Mass ····· 10

Table 2. Az values difference of conventional CT alone Versus the combination of CT and perfusion CT ····· 10

Table 3. Sensitivity and specificity in Differential diagnosis of cavitary mass with conventional CT alone versus the combination of CT and perfusion CT ····· 10

Abbreviations

CI	Confidence Interval
CT	Computed Tomography
MDCT	Multidetector Computer Tomography
MER	Maximum Enhancement Ratio
MR	Magnetic Resonance
ROI	Region of Interest
TB	Tuberculosis
TBLB	Transbronchial Lung Biopsy
TTP	Time to Peak

Abstract

Lung Perfusion CT:
The Differentiation of Cavitary Mass

Young Han Lee
Department of Medicine
The Graduate School, Yonsei University

PURPOSE: To evaluate lung perfusion maps based on region of interest (ROI)-studies in the differentiation of cavitary mass.

MATERIALS AND METHODS: Fifty-three patients with cavitary lung masses who underwent dynamic chest computed tomography (CT) with lung perfusion protocol were analyzed. All patients underwent a biopsy to confirm the diagnosis. Dynamic chest CT was performed prior to and at 15, 30, 45, 60, 90, 120, 180, and 300 seconds (from the thoracic inlet to the adrenal gland) at 60 seconds after contrast medium injection. The volume map, washout map, peak map, and time-to-peak map were reformatted using IDL (Interactive Data Language). The perfusion patterns were classified into three scoring groups, and these scorings was repeated after 2-week intervals. Diagnostic confidence levels were assigned by consensus.

McNemar's chi-square test was used to determine interobserver agreement, and Fisher's exact test was used to analyze statistical differences in perfusion

scores. Receiver operating characteristic (ROC) analysis was performed to evaluate the usefulness of the perfusion maps

RESULTS: Volume maps, washout maps, peak maps, and time-to-peak (TTP) maps were reformatted pixel-by-pixel from the time-to-intensity curve analyses using post-processing software made in-house, and these maps showed perfusion values at a glance. Of 23 patients with pyogenic cavities, 16 (69.6%) showed weak washout and slow TTP. Conversely, of 15 patients with malignant cavities, 11 (73.3%) showed strong washout. Of 15 patients with tuberculous cavities, 9 (66.7%) showed low perfusions in the volume and peak maps. Interobserver agreement was excellent for each parameter. The performance of the combination of CT and the perfusion map was always better than that of CT alone (Az value differences, 0.132, 0.163, 0.167; significance levels, $p<0.040$, $p<0.020$, $p<0.042$, respectively).

CONCLUSION: Lung perfusion CT could be a promising and feasible method for differentiation of cavitary mass. Thus, it could be very beneficial for the noninvasive diagnosis of cavitary masses, as well as for proper therapeutic planning.

Key words : Cavitation, Lung, Thorax, CT perfusion, CT

Lung Perfusion CT:
The Differentiation of Cavitary Mass

Young Han Lee

Department of Medicine
The Graduate School, Yonsei University

Directed by Professor Myung Soon Kim

I. Introduction

Information about the morphologic features of a cavitary mass on computed tomography (CT) scans may be insufficient provide an accurate and early diagnosis, and differentiation of a cavitary lung mass is still radiologically and clinically problematic. Morphologic observations such as wall thickness, eccentricity, air-fluid level, the presence of multiple cavities in one mass, and marginal irregularity would help differentiate benign and malignant cavities when they have typical features (1), but there is considerable overlap in the morphologic presentation of many cases in clinical daily practice.

Findings in recent studies using dynamic CT or magnetic resonance (MR) with manually-defined regions of interest (ROIs) indicate that differentiation between benign and malignant nodules is feasible (2-13). However, these studies using manual ROI have some limitations including: the need for additional time-consuming tasks, operator-dependency, poor reproducibility, the absence of a parametric perfusion map at a glance, and questionable feasibility in daily practice.

For that reason, we postulated that mapping perfusion values from dynamic CT images after injecting intravenous contrast medium would be a helpful and useful diagnostic tool for differentiation of cavitary mass. Thus, as previous reports based on dynamic studies have demonstrated, we attempted to reconstruct perfusion CT maps including the volume map, washout map, peak map, and time-to-peak (TTP) map. The purposes of this study were to assess the findings of perfusion CT maps in cavitary masses and to evaluate the usefulness of perfusion CT, with a focus on differentiating pyogenic, tuberculous, and malignant cavitary mass.

II. Materials and Methods

2.1. Patients selection

Cases from fifty-three patients with cavitary lung masses who underwent dynamic chest CT scans with lung perfusion CT protocol between September 2005 and March 2007 were examined retrospectively. All patients underwent lung perfusion CT before biopsy. All patients' diagnoses were confirmed with transbronchial lung biopsy (TBLB) or CT-guided transthoracic needle biopsy.

The patients ranged in age from 28 to 84 years (mean age, 60.4 years); 41 were men and 12 were women. Of these patients 23 had pyogenic cavities, 15 had tuberculous cavities, and the remaining 15 had malignant cavities. The last group consisted of squamous cell carcinoma (n=9), adenocarcinoma (n=5), and metastatic squamous cell carcinoma (n=1).

No specific approval by our institutional review board is needed for retrospective studies. Excluded from the study were cases demonstrating poor cooperation, previous chemotherapy, cavitary masses that were too small, and excess motion artifacts.

2.2. Methods

2.2.1. Dynamic CT imaging studies

All the source images of lung perfusion CT were obtained with 16-channel MDCT (LightSpeed Pro 16; GE Medical Systems, Milwaukee, WI). An

18-gauge cannula was placed into an antecubital fossa vein while the patient lay supine on the scanner table. The following imaging parameters were used: 120 kV; 200 mAs; table feed, 13.75 mm; matrix, 512 x 512. All studies were performed using breath-hold with full inspiration.

Before the intravenous injection of contrast medium, a series of 10 images was obtained throughout the nodule for 25 mm along the z-axis with 2.5-mm collimation. This precontrast study provided a baseline image and was used to plan the subsequent perfusion study. Thereafter, an additional eight series of images were obtained at 0, 15, 30, 45, 60, 90, 120, 180, and 300 seconds (throughout the mass for 25 mm along the z-axis [10 images], and from thoracic inlet to adrenal gland) at 60 seconds after injecting contrast medium (4 mL/sec, total of 120 mL of nonionic iodide contrast, Ultravist® 300; Schering, Seoul, Korea) with a power injector (Stellant Dual®; Medrad, Indianola, PA) with the same parameters as for the initial precontrast series (9 total series of images obtained at 0, 15, 30, 45, 60, 90, 120, 180, and 300 seconds).

2.2.2. Lung perfusion maps

Image reconstruction and perfusion mapping were performed on a separate IBM compatible personal computer, using dedicated image-reconstruction software made in-house using Interactive Data Language (IDL; Research Systems Inc., Boulder, CO) as a development tool. The volume map, washout map, peak map, and TTP map were reformatted pixel-by-pixel from time-to-intensity curve analysis using post-processing software. For each pixel, the change in Hounsfield Units (HUs) over time after contrast material

administration was transformed by a model-independent method to generate color-coded parametric maps of volume, washout, peak, and TTP maps for the cavitary mass (Fig 1). Each pixel location within the perfusion map corresponded to a single semiquantitative perfusion value that resulted from the mathematical calculation of the data at that pixel (i.e., perfusion maps were created on a pixel-by-pixel basis). This lung perfusion processing was automated, eliminating operator-dependent errors.

2.2.3. Image Analysis

All the perfusion CT maps and conventional images were interfaced to our personal computer, which displayed all image data on a monitor (1280 x 1024 resolution and 24-bit colors). The first analysis is a perfusion pattern analysis to evaluate the differences in perfusion CT maps and to show the trends in perfusion CT maps, and the second analysis is a confidence scale analysis to compare the diagnostic performance of the perfusion CT maps with that of conventional CT. All the conventional CT and perfusion CT maps were reviewed independently by two chest radiologists unaware of the clinical information or histopathologic data.

First, the perfusion patterns were classified into three scores (high perfusion, 3; intermediate perfusion, 2; low perfusion, 1) as follows: high, middle, and low perfusion on volume and peak maps; intense, intermediate, and weak washout on washout maps; and fast, intermediate, and slow perfusion on time-to-peak maps. The final scorings for the CT perfusion findings were reached by consensus.

Second, the image review consisted of two sessions: conventional CT alone

and the combination of CT and perfusion maps. Diagnostic confidence levels (1= definitely negative, 2= possibly negative, 3=equivocal, 4=possibly positive, 5= definitely positive) were assigned by two chest radiologists who were unaware of the clinical information or histopathologic data. The final confidence levels were reached by consensus.

A review of conventional CT alone was performed. These conventional CT scans comprised two images per patient: mediastinal window (window width, 400 HU; window level, 30 HU) and lung window (window width, 1600 HU; window level, －700 HU) images at the same level of the perfusion maps. Diagnostic confidence levels with conventional CT were assigned by two chest radiologists who were unaware of the perfusion CT findings. Reviewers focused on the findings for the cavitary masses, which included wall thickness, inner and outer margins, eccentricity, and air-fluid level. We did not consider any ancillary findings, such as satellite nodules, lymphadenopathy, metastasis, and pleural effusion. Thereafter, review of the perfusion CT maps was performed at 2-week intervals to minimize learning and recall biases. Lung perfusion CT scans were evaluated to differentiate the cavitary masses by assigning diagnostic confidence levels regarding the likelihood of pyogenic, tuberculous, or malignant cavitary masses using the continuous 5-point rating scale.

2.2.4. Statistical Analysis

The interobserver agreement between two reviewers for perfusion level was calculated with McNemar’s chi-square test. As previously suggested (14), a kappa statistic greater than 0.75 was considered to indicate excellent agreement

beyond chance; 0.4-0.75 indicated fair to good agreement; and less than 0.4 indicated poor agreement. The Fisher's exact test was used to analyze statistical differences in perfusion scores among pyogenic, tuberculous, and malignant groups of patients who underwent dynamic lung perfusion CT.

Receiver operating characteristic (ROC) analysis was performed to evaluate the usefulness and diagnostic performance of perfusion maps compared with those of conventional CT alone. Each area under the ROC curve (Az) was calculated. Descriptive statistical analysis was performed as follows: sensitivity and specificity for each diagnostic modality were calculated using a confidence rating of 4 or 5 as positive.

A p value of less than 0.05 was considered to indicate a statistically significant difference. ROC analysis was performed using MedCalc software (version 7.4, Mariakerke, Belgium). All other statistical analyses were performed with SPSS software (version 11.0; SPSS Inc., Chicago, IL).

III. Results

3.1. Lung CT perfusion features

The volume map, washout map, peak map, and TTP map were reformatted pixel-by-pixel from the time-to-density curve analysis using a post-processing software made in-house, and these perfusion maps showed the perfusion values of the cavities at a glance by differences in spectra of colors (Fig 3-7).

Perfusion scorings in pyogenic, tuberculous, and malignant cavities were statistically different in volume, washout, peak map, and TTP map ($p = 0.002$, $p = 0.001$, $p = 0.001$, $p = 0.001$, respectively). The volume maps of pyogenic cavities showed significantly higher perfusion than those of malignant and tuberculous cavities ($p = 0.001$). Washout maps of malignant cavities showed significantly higher perfusion (i.e. intense washout) than those of benign (pyogenic and tuberculous) cavities ($p = 0.002$). Tuberculous cavities showed low perfusions in the volume, peak map, and washout maps.

Of 23 patients with pyogenic cavities, 16 (69.6%) showed weak washout and slow TTP. Conversely, of 15 patients with malignant cavities, 11 (73.3%) showed strong washout. Of 15 patients with tuberculous cavities, 10 (66.7%) showed low perfusion in the volume and peak maps (Table 1).

3.2. Interobserver agreement

Interobserver agreement was excellent for each parameter as indicated by a kappa of 0.770 (p=0.001), 0.854 (p=0.001), 0.781 (p=0.001), and 0.822 (p=0.001) for volume maps, washout maps, peak maps, and TTP maps,

respectively.

3.3. ROC Analysis

The areas under the ROC curves for pyogenic, tuberculous, and malignant cavities were as follows: 0.820 (95% CI, 0.690 to 0.911) for CT alone, and 0.952 (95% CI, 0.855 to 0.991) for the combination of CT and perfusion maps; 0.816 (95% CI, 0.685 to 0.909) for CT alone, and 0.979 (95% CI, 0.895 to 0.997) for the combination of CT and perfusion maps; and 0.767 (95% CI, 0.630 to 0.872) for CT alone, and 0.934 (95% CI, 0.831 to 0.983) for the combination of CT and perfusion maps, respectively. The performance of the combination of CT and perfusion map was always better than that of CT alone (Az value differences, 0.132, 0.163, 0.167; significance levels, $p<0.040$, $p<0.020$, $p<0.042$, respectively). (Tables 2, 3; Fig 2).

Table 1. CT perfusion characteristics of Cavitary Mass

	Abscess (n=23)	Tuberculosis (n=15)	Malignancy (n=15)
Volume map	H(17/23)	L(10/15)	H(9/15)
Washout map	L(16/23)	L(6) or I(7)	H(11/15)
Peak map	H(19/23)	L(6) or I(5)	H(12/15)
TTP map	H(20/23)	I (11)	L(6) or I(8)

TTP = Time-to-peak, H = high perfusion , I = intermediate perfusion, L=low perfusion

Table 2. Az values difference of conventional CT alone Versus the combination of CT and perfusion CT

	ROC Performance (Az)		
	Pyogenic	Tuberculosis	Malignancy
CT alone	0.820	0.816	0.767
Perfusion CT	0.952	0.979	0.934
P value	0.040	0.020	0.042

Table 3. Sensitivity and specificity in Differential diagnosis of cavitary mass with conventional CT alone versus the combination of CT and perfusion CT

	Sensitivity (%)			Specificity (%)		
	Pyogenic	TB	Malignancy	Pyogenic	TB	Malignancy
CT alone	73.9	73.3	80.0	90.0	86.8	65.8
Perfusion CT	95.7	80.0	73.3	93.3	100.0	89.5

TB = Tuberculosis

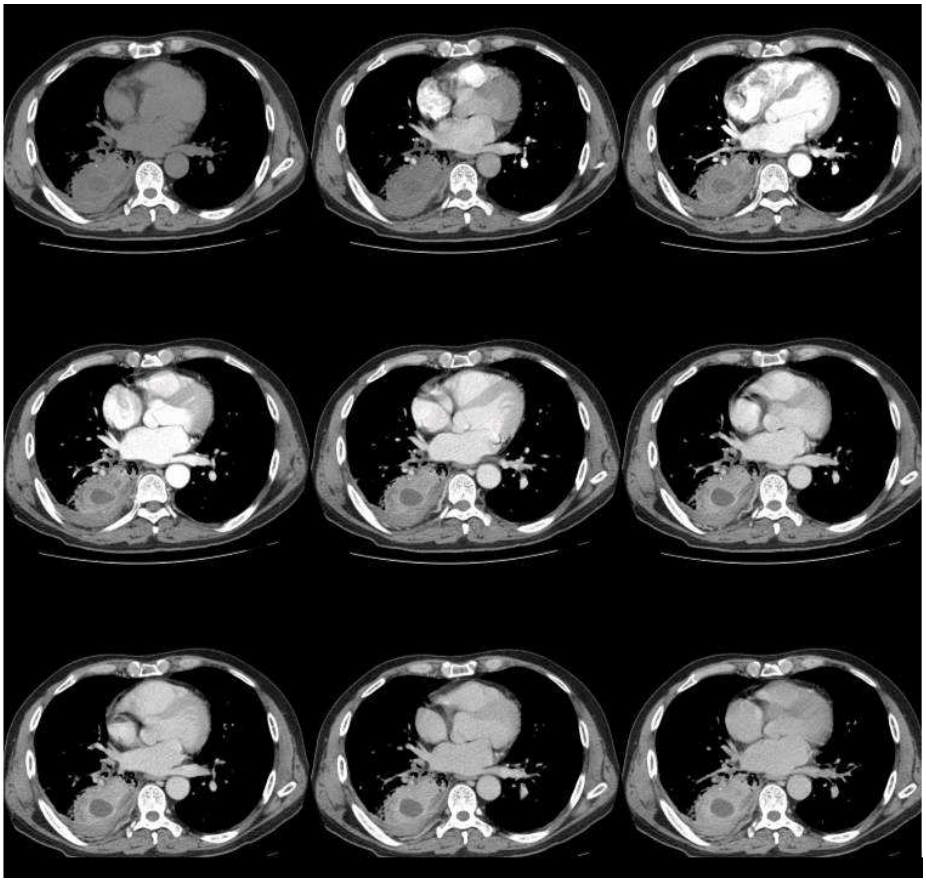

Figure 1. Perfusion source images.

Dynamic CT source images in a 55-year-old man with a lung abscess on the right lower lobe. The source image set consists of nine serial dynamic images. This nodule was 22 x 24 mm in diameter. Note placement of region of interest (ROI). Nine total series of images obtained at 0, 15, 30, 45, 60, 90, 120, 180, and 300 seconds.

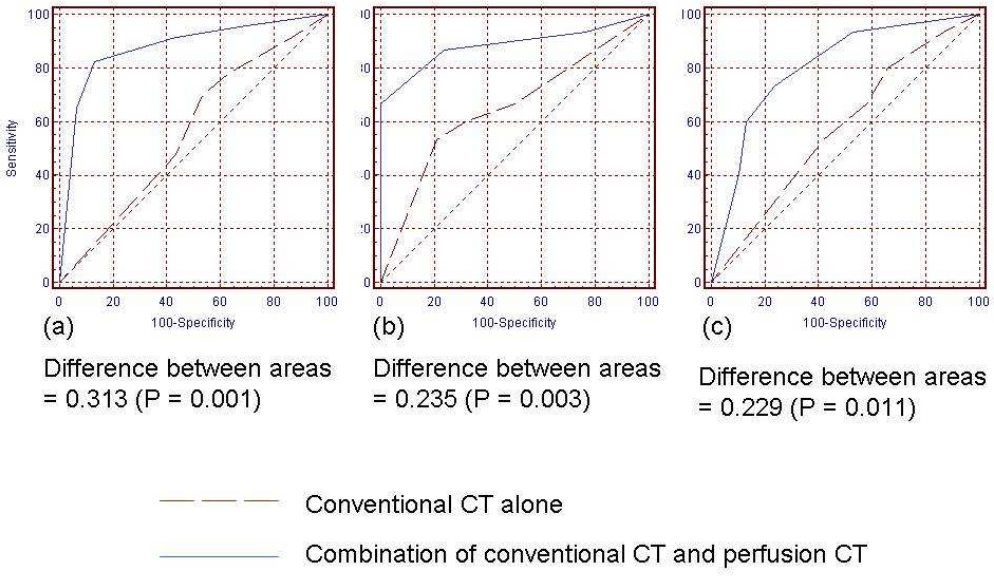

Figure 2. Graphs of the ROC curves for cavitary masses.

(a) ROC curves for inflammatory cavities. The Az values are 0.820 (95% CI, 0.690 to 0.911) for CT alone and 0.952 (95% CI, 0.855 to 0.991) for the combination of CT and perfusion maps. The difference between the two areas is 0.132 (P = 0.040).

(b) ROC curves for tuberculous cavities. The Az values are 0.816 (95% CI, 0.685 to 0.909) for CT alone and 0.979 (95% CI, 0.895 to 0.997) for the combination of CT and perfusion maps. The difference between the two areas is 0.163 (P = 0.020).

(c) ROC curves for malignant cavities. The Az values are 0.767 (95% CI, 0.630 to 0.872) for CT alone and 0.934 (95% CI, 0.831 to 0.983) for the combination of CT and perfusion maps. The difference between the two areas is 0.167 (P = 0.042).

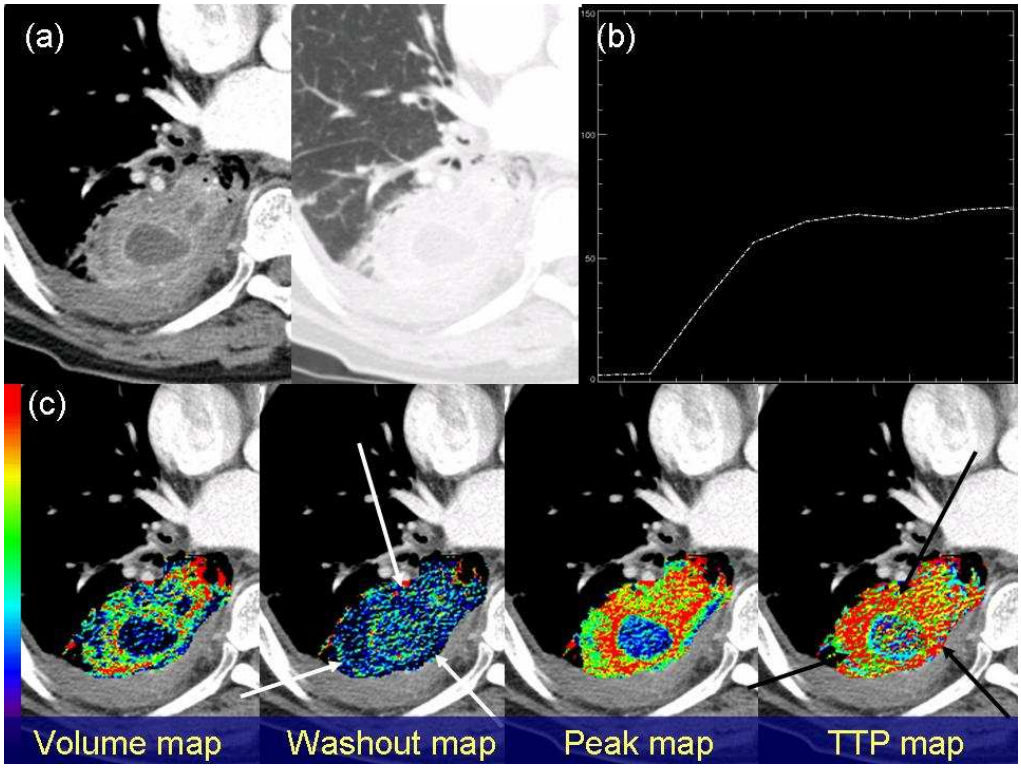

Figure 3. Chest CT and parametric perfusion maps in a 55-year-old man with a lung abscess in the right lower lobe superior segment.

(a) Mediastinal and lung window setting of transverse thin-section (2.5-mm collimation) CT scan obtained at the level of the right superior pulmonary vein shows an irregular thick-walled cavitary mass. This mass contained central low density. Ipsilateral pleural effusion is noted.

(b) A continuous increase of attenuation following intravenous administration of contrast material demonstrates a gradually increased pattern in time-concentration curves.

(c) Four parametric perfusion maps, including volume map, washout map, peak map, and TTP (time-to-peak) map, were reformatted at the same level. Volume map and peak map show red and yellow colors signifying high perfusion. Washout map shows blue and cyan colors signifying weak washout (white arrows). TTP map shows red color signifying slow and prolonged flow (black arrows).

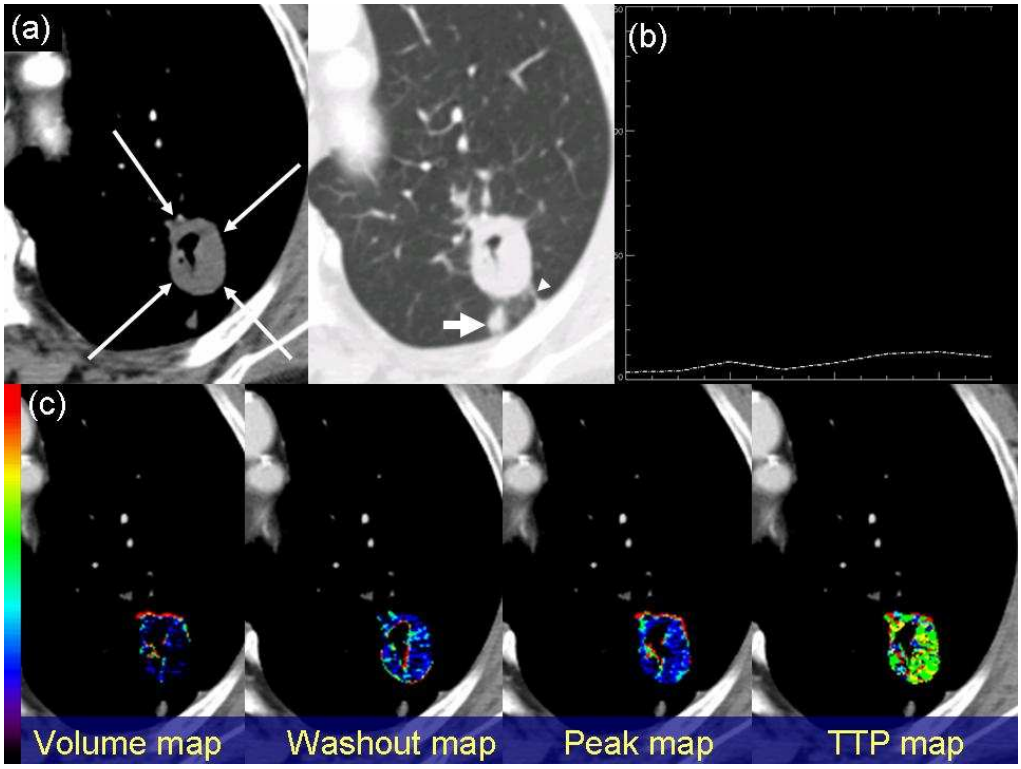

Figure 4. Chest CT and parametric perfusion maps in a 63-year-old woman with tuberculosis in the left upper lobe apicoposterior segment.

(a) Mediastinal and lung window setting of transverse thin-section (2.5-mm collimation) CT scan shows an approximately 3.0-cm-sized cavitary mass (arrows) with a satellite nodule (thick arrow) and a pleural tag (arrowhead).

(b) This curve demonstrates a plateau. No relevant enhancement was calculated after intravenous administration of contrast material.

(c) Four parametric perfusion maps, including volume map, washout map, peak map, and TTP (time-to-peak) map, were reformatted at the same level. The volume map and peak map show blue color signifying low perfusion. The washout map shows blue color signifying weak washout. The TTP map shows yellow and green colors signifying relatively slow flow.

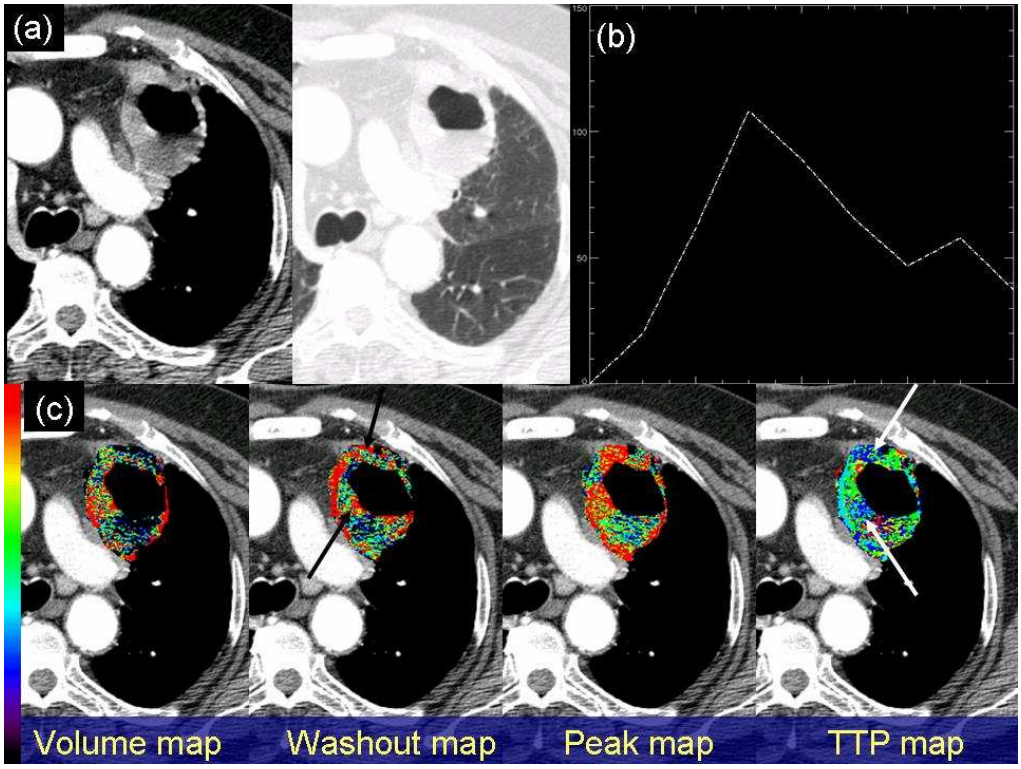

Figure 5. Chest CT and parametric perfusion maps in a 35-year-old man with squamous cell carcinoma in the left upper lobe apicoposterior segment.

(a) Mediastinal and lung window setting of transverse thin-section (2.5-mm collimation) A CT scan obtained at the level of the left pulmonary artery shows an approximately 5.1-cm-sized, relatively thin-walled cavitary mass with air-fluid level.

(b) This curve was characterized by a fast density increase and an obvious decrease after the first bolus transit. The second peak was due to secondary circulation.

(c) Four parametric perfusion maps, including volume map, washout map, peak map, and TTP (time-to-peak) map, were reformatted at the same level. The volume map and peak map show red and green colors signifying relatively high perfusion. The washout map shows red color (black arrows) signifying focal intense washout, which is explained by washout. TTP map shows a tiny focal fast flow, which indicates intense washout on the washout map, showing a sky blue color (white arrows).

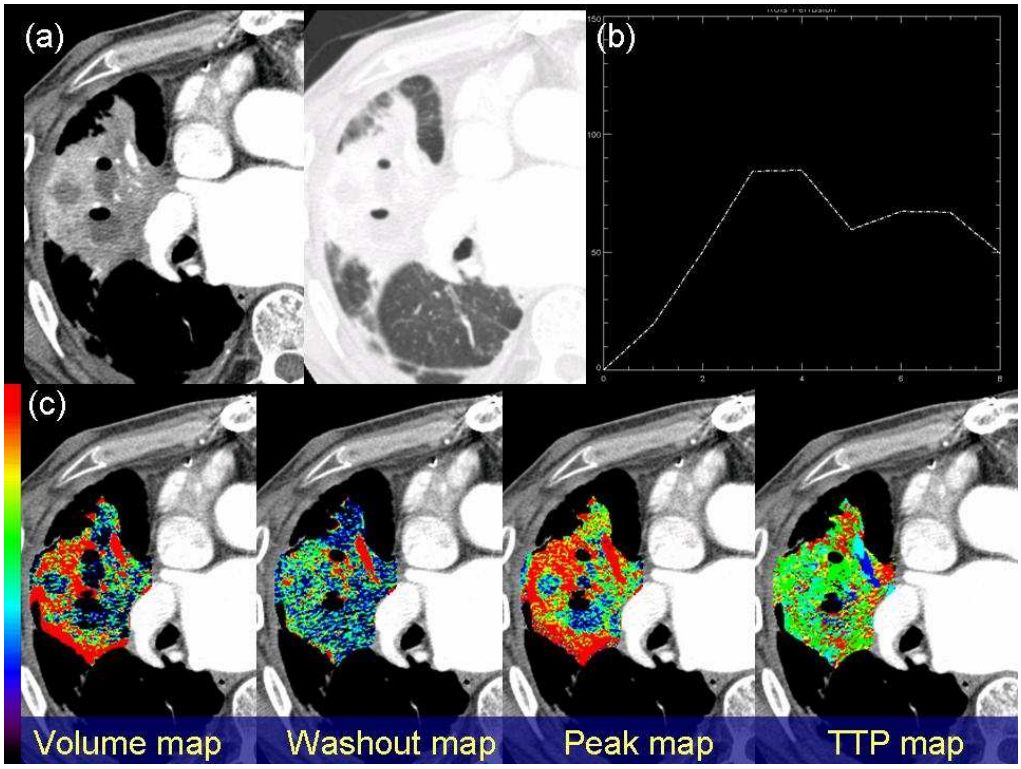

Figure 6. Chest CT and parametric perfusion maps in a 55-year-old man with squamous cell carcinoma in the right upper lobe.

(a) Mediastinal and lung window setting of transverse thin-section (2.5-mm collimation) CT scan obtained at the level of the right superior pulmonary vein shows an approximately 8.1-cm-sized heterogeneous multicavitated mass with an infiltrating margin.

(b) This curve was characterized by a fast density increase and an obvious decrease after the first bolus transit.

(c) Four parametric perfusion maps including volume map, washout map, peak map, and TTP (time-to-peak) map were reformatted at the same level. The volume map and peak map show red and green colors signifying relatively high perfusion. The washout map shows red color signifying intense washout, which is explained by washout. The TTP map shows green and sky blue colors signifying relatively fast flow.

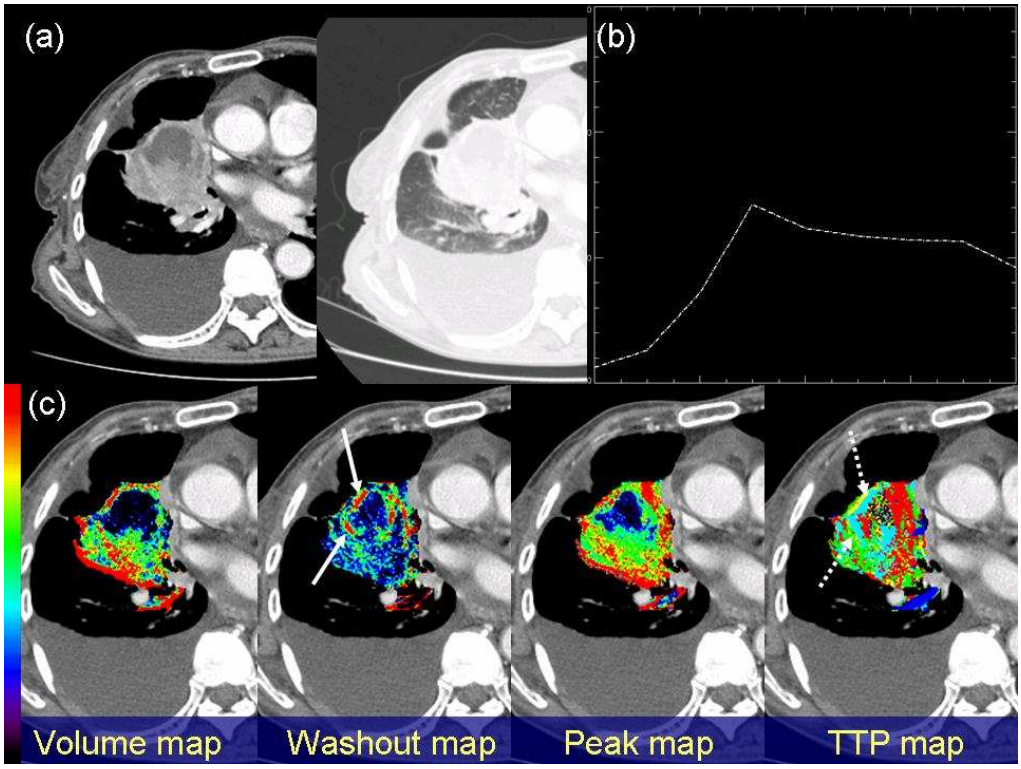

Figure 7. Chest CT and parametric perfusion maps in a 71-year-old woman with adenocarcinoma in the right middle lobe.

(a) Mediastinal and lung window setting of transverse thin-section (2.5-mm collimation) CT scan shows an approximately 5.3 x 5.1-cm-sized mass with necrotic portions.

(b) This curve was characterized by a fast density increase and an obvious decrease after the first bolus transit.

(c) Four parametric perfusion maps, including volume map, washout map, peak map, and TTP (time-to-peak) map, were reformatted at the same level. The volume map and peak map show red and green color signifying relatively high perfusion. The washout map shows red color signifying intense washout (white arrows), which is explained by washout. The TTP map shows green and sky blue colors signifying fast flow (dashed arrows).

IV. Discussion

The differential diagnosis of a cavitary mass is clinically and radiologically important for the determination of treatment planning and prediction of the patient's outcome. The presence of cavitation in lung cancer is common and has been reported in 2–16% of lung cancer patients (15). Known CT features suggestive of a malignant cavity include wall thickness over 4 mm and spiculated or irregular margins of inner and outer cavity walls. The tuberculous cavity is a common feature suggestive of active status in tuberculosis patients. Hadlock et al. (16) reported that 120 (51%) patients among 236 had evidence of cavitation, and Woodring et al. (17) demonstrated that tuberculous cavitation was common (45%) with various cavity wall thicknesses (from very thin and smooth to very thick and nodular). A lung abscess is defined as a localized area of suppuration with destruction of lung parenchyma (18). The conventional CT features of an abscess include irregular inner (57%) and outer margins (91%), relatively thin walls (mean 1.0cm), central location (57%), and air-fluid level (86%) (1). Morphologic evaluation would help differentiate these cavitary masses when they have typical features, but there is considerable overlap in morphologic presentation in many cases.

Some authors have reported the usefulness of contrast-enhanced dynamic CT in the work-up of solitary pulmonary nodules (SPNs) (4-12, 19-20). Recent technological advances in helical multidetector CT (MDCT) allow precise evaluations of hemodynamic characteristics in tissue. Findings in recent studies using manually-defined ROI (Regions of Interest) indicate that enhancement of

malignant SPNs following intravenous administration of contrast material is greater than that of benign SPNs depicted on CT scans and MR images (2-3, 8, 13, 21). Schaefer et al. (22) simplified the findings into four distinct signal intensity profiles: fast initial increase and marked decrease, fast initial increase and no decrease, continuous increase, and no relevant enhancement. Signal intensity changes in dynamic MR parameters such as MER, slope, and washout ratio correlate with tumor vascularity, and these dynamic MR parameters may be helpful in the prediction of prognosis, as described in the study of Fujimoto et al. (23). Yi et al. (2) reported that the extent of enhancement reflects underlying nodule angiogenesis using net enhancement, maximum enhancement ratio (MER), time to peak (TTP), and slope. However, these studies using manually-defined ROI have some limitations, including the need for additional time-consuming tasks, operator-dependency, poor reproducibility, the absence of a parametric perfusion map at a glance, and questionable feasibility in daily practice. Parametric perfusion maps can be reformatted pixel-by-pixel from time-to-intensity curves on the basis of previous ROI studies. Interest in lung perfusion maps has been growing. Recently, an MDCT technique was shown to permit quantitative whole tumor perfusion assessment, and good measurement reproducibility for lung masses was reported (24).

In the present study, we used various acquisition time intervals (15, 30, 45, 60, 90, 120, 180, and 300 seconds) to obtain dynamic information about cavitary masses. These intervals enabled us to obtain a suitable and acceptable time-to-density curve by identifying the detailed changes in HU for the entire

duration of dynamic imaging. Furthermore, we could reconstruct four perfusion maps in an automated fashion, eliminating human bias in manually defining ROI. These perfusion maps provide various perfusion values at a glance by differences in spectra of colors. The perfusion patterns were classified into three scores as follows: high, middle, and low perfusion in volume and peak maps; intense, intermediate, and weak washout in washout maps; and fast, intermediate, and slow perfusion in time-to-peak maps. By using this scoring system, the complex and various perfusion maps could be simplified, and assessment of the perfusion maps can be made easier.

In our study, the walls of pyogenic cavities showed a characteristic finding (16 of 23 pyogenic cavities; 69.6%): weak washout on the washout map (blue and cyan colors) and slow flow on the TTP map (red and yellow colors) (Fig 3). Our study population contained only one patient with a pyogenic cavity that may have shown rapid washout on the washout map. The TTP map showed slow and prolonged perfusion in 20 patients among a total of 23 patients who had pyogenic cavities. An histopathologic finding associated with an abscess is an abundant formation of granulation and fibrosis, which implies a regenerative healing process associated with inflammation. In the present study, we expected that abundant formation of granulation and fibrosis would reflect characteristic perfusion findings.

We observed some interesting features of perfusion in the walls of tuberculous cavities: significant low perfusions (blue and cyan colors) were shown in the peak and volume maps after contrast medium injection (10 of 15 tuberculous cavities; 66.7%). On the other hand, the washout maps and TTP maps showed nonspecific patterns (Fig 4). The wall of the tuberculous cavity

consists of caseous materials, epithelioid cells with multinucleated giant cells, granulation tissue, and a fibrous capsule (25). The enhancing area corresponds histopathologically to a fibrous capsule or epithelioid granulomas in a remnant of granulation tissue, whereas a nonenhancing area corresponds to a caseous or liquefied necrotic area (26). In the present study, we thought these fibrous capsules or epithelioid granulomas would be depicted as significant low perfusions.

The walls of malignant cavities were characterized by washout maps (11 of 15 malignant cavities; 73.3%), similar to those of ROI studies (2-3, 27-28). Of 15 patients with malignant cavities, 6 (40%) showed strong and rapid washout and fast TTP, and 12 (80%) showed high perfusion in peak maps (Fig 5-7). This washout phenomenon of contrast material has been seen in a variety of other tumor types with signs of hypervascularity (27). This type of washout is known to correlate with the tumor interstitium (the density grade of elastic fibers and collagen fibers, elastic fibers 1-3 and collagen fibers 1-3) (23). This strong contrast enhancement and rapid washout is related to high vascularity in tumors and interstitial accumulation of contrast material by means of increased permeability of tumor capillaries (28). These features are often present in malignant tumors (29-31). However, another study reported that no parenchymal destruction or tumor-associated neovascularization was found in 16% of 500 stage I primary lung cancers (32). In addition, pyogenic conditions have been demonstrated to stimulate an increased blood flow in malignant lesions (3, 11, 33). In our study, high perfusions were seen in 12 of 15 patients (80%) with malignant cavities and 19 of 23 patients (82.6%) with pyogenic cavities. Therefore, we thought that the strong enhancement (i.e.

high perfusion on the peak map) is not sufficient to indicate malignancy. However, rapid washout could be a reliable finding for differential diagnosis.

In our study, ROC analysis was used to evaluate the usefulness of perfusion maps, compared with conventional CT alone for differentiating cavitary masses. The performance of the combination of CT and perfusion maps was always better than that of CT alone (Fig 2). In other words, differentiations of cavitary masses were more easily achieved with a combination of CT and perfusion maps than with chest CT alone with statistical significance (Az value difference, 0.313, 0.235, 0.229; significance level, p=0.001, p=0.003, p=0.011, respectively). On the other hand, the sensitivity of CT alone is higher than that of the combination of CT and perfusion maps in differentiating malignant cavities. We thought that this might be due to the tendency to overread the cavitary mass in uncertain cases (Table 3).

Our study has the following limitation: on conventional CT review, we focused on the features of the cavity in the present study, but we did not consider any ancillary findings including satellite nodules, lymphadenopathy, metastasis, and pleural effusion. So there may be a difference between the evaluation in our study and readings in clinical daily practice.

V. Conclusion

In conclusion, lung perfusion CT could be a promising and feasible method for assessing cavitary mass. Thus, it could be very beneficial in allowing for noninvasive diagnoses of cavitary mass and in planning the proper therapeutic planning.

References

1. Lee YR, Kim MG, Kang EY, Suh WH. CT evaluation of cavitary lung lesions: focused on lung cancer, tuberculosis and abscess. Journal of the Korean Radiological Society 1992;28:897-902.

2. Yi CA, Lee KS, Kim EA, et al. Solitary pulmonary nodules: dynamic enhanced multi-detector row CT study and comparison with vascular endothelial growth factor and microvessel density. Radiology 2004;233:191-199.

3. Zhang M, Kono M. Solitary pulmonary nodules: evaluation of blood flow patterns with dynamic CT. Radiology 1997;205:471-478.

4. Swensen SJ, Brown LR, Colby TV, Weaver AL. Pulmonary nodules: CT evaluation of enhancement with iodinated contrast material. Radiology 1995;194:393-398.

5. Yamashita K, Matsunobe S, Tsuda T, et al. Solitary pulmonary nodule: preliminary study of evaluation with incremental dynamic CT. Radiology 1995; 194:399-405.

6. Yamashita K, Matsunobe S, Takahashi R, et al. Small peripheral lung carcinoma evaluated with incremental dynamic CT: radiologic-pathologic correlation. Radiology 1995;196:401-408.

7. Swensen SJ, Brown LR, Colby TV, Weaver AL, Midthun DE. Lung nodule enhancement at CT: prospective findings. Radiology 1996;201:447-455.

8. Swensen SJ, Viggiano RW, Midthun DE, et al. Lung nodule enhancement at CT: multicenter study. Radiology 2000;214:73-80.

9. Semelka RC, Maycher B, Shoenut JP, Kroeker R, Griffin P, Lertzman M. Dynamic Gd-DTPA enhanced breath-hold 1.5 T MRI of normal lungs and patients with interstitial lung disease and pulmonary nodules: preliminary results. Eur Radiol 1992;2:576-582.

10. Kono M, Adachi S, Kusumoto M, Sakai E. Clinical utility of Gd-DTPA-enhanced magnetic resonance imaging in lung cancer. J Thorac Imaging 1993;8:18-26.

11. Hittmair K, Eckersberger F, Klepetko W, Helbich T, Herold CJ. Evaluation of solitary pulmonary nodules with dynamic contrast-enhanced MR imaging: a promising technique. Magn Reson Imaging 1995;13:923-933.

12. Gückel C, Schnabel K, Delmling M, Steinbrich W. Solitary pulmonary nodules: MR evaluation of enhancement patterns with contrast-enhanced dynamic snapshot gradient-echo imaging. Radiology 1996;200:681-686.

13. Schaefer JF, Schneider V, Vollmar J, et al. Solitary pulmonary nodules: association between signal characteristics in dynamic contrast enhanced MRI

and tumor angiogenesis. Lung Cancer. 2006;53:39-49.

14. Landis JR, Koch GG. The measurement of observer agreement for categorical data. Biometrics. 1977;33:159-174.

15. Felson B, Wiot JF. Some less familiar roentgen manifestations of carcinoma of the lung. Semin Roentgenol. 1977;12:187-206.

16. Hadlock FP, Park SK, Awe RJ, Rivera M. Unusual radiographic findings in adult pulmonary tuberculosis. AJR Am J Roentgenol. 1980;134:1015-1018.

17. Woodring JH, Vandiviere HM, Fried AM, Dillon ML, Williams TD, Melvin IG. Update: the radiographic features of pulmonary tuberculosis. AJR Am J Roentgenol. 1986;146:497-506.

18. Alexander JC Jr, Wolfe WG. Lung abscess and empyema of the thorax. Surg Clin North Am 1980;60:835-849.

19. Yamashita K, Matsunobe S, Tsuda T, et al. Solitary pulmonary nodule: preliminary study of evaluation with incremental dynamic CT. Radiology 1995;194:399-405.

20. Swensen SJ, Morin RL, Schueler BA, et al. Solitary pulmonary nodule: CT evaluation of enhancement with iodinated contrast material. Radiology 1992;182:343-347.

21. Kono R, Fujimoto K, Terasaki H, et al. Dynamic MRI of Solitary Pulmonary Nodules: Comparison of Enhancement Patterns of Malignant and Benign Small Peripheral Lung Lesions. AJR Am J Roentgenol. 2007;188:26-36.

22. Schaefer JF, Vollmar J, Schick F, et al. Solitary pulmonary nodules: dynamic contrast-enhanced MR imaging-perfusion differences in malignant and benign lesions. Radiology 2004;232:544-553.

23. Fujimoto K, Abe T, Muller NL, et al. Small peripheral pulmonary carcinomas evaluated with dynamic MR imaging: correlation with tumor vascularity and prognosis. Radiology. 2003;227:786-793.

24. Ng QS, Goh V, Fichte H, et al. Lung cancer perfusion at multi-detector row CT: reproducibility of whole tumor quantitative measurements. Radiology. 2006;239:547-553.

25. Lee JY, Lee KS, Jung KJ, et al. Pulmonary tuberculosis: CT and pathologic correlation. J Comput Assist Tomogr. 2000;24:691-698.

26. Murayama S, Murakami J, Hashimoto S, Torii Y, Masuda K. Noncalcified pulmonary tuberculomas: CT enhancement patterns with histologic correlation. J Thorac Imaging. 1995;10:91-95.

27. Liberman L, Morris EA, Lee MJ, et al. Breast lesions detected on MR

imaging: features and positive predictive value. AJR Am J Roentgenol. 2002;179:171-178.

28. Dean PB, Niemi P, Kivisaari L, Kormano M. Comparative pharmacokinetics of gadolinium DTPA and gadolinium chloride. Invest Radiol. 1988;23(suppl 1):S258-S260.

29. Abramovitch R, Marikovsky M, Meir G, Neeman M. Stimulation of tumour angiogenesis by proximal wounds: spatial and temporal analysis by MRI. Br J Cancer 1998;77:440-447.

30. Chambers JS. Angiogenesis in lung cancer. Ann Thorac Surg 1998; 66:2162-2163.

31. Cox G, Jones JL, Walker RA, Steward WP, O'Byrne KJ. Angiogenesis and non‐small cell lung cancer. Lung Cancer 2000;27:81-100.

32. Pezzella F, Pastorino U, Tagliabue E, et al. Non‐small-cell lung carcinoma tumor growth without morphological evidence of neo-angiogenesis. Am J Pathol. 1997;151:1417-1423.

33. Ohno Y, Hatabu H, Takenaka D, Adachi S, Kono M, Sugimura K. Solitary pulmonary nodules: potential role of dynamic MR imaging in management - initial experience. Radiology 2002;224:503-511.

Abstract in Korean

폐 관류 CT: 공동성 종괴의 감별

Lung Perfusion CT: The Differentiation of Cavitary Mass

<지도교수 김 명 순>

연세대학교 대학원 의학과

이 영 한

목적: 관심영역을 이용한 연구들을 기반으로 하여 공동성 종괴 감별에서 폐 관류 CT의 유용성을 평가하고자 하였다.

대상과 방법: 단순 촬영에서 공동성 종괴를 가진 53명의 환자를 대상으로 관류 CT 소견을 분석하였다. 역동적 관류 CT 영상 자료를 얻기 위해서 16열 다중 검출기 CT를 사용하였고 다중 나선식 획득방식으로 조영 전 영상과 조영제 주입 후 15초, 30초, 45초, 60초, 90초, 120초, 180초, 300초에 촬영하여 원시영상을 얻었다. 개발도구로는 IDL(Interactive Data Language)을 이용하여 Volume map, Washout map, Peak map, 그리고 Time-to-peak(TTP) map을 구현하였다. 관류 지도를 육안적 분석으로 점수화하였으며 멕네마르 카이스퀘어 검정(McNemar's chi-square test)을 이용한 일치도를 확인하였다. 각 관류지도의 점수는 피셔 정확 검정(Fisher's exact test)을 이용하여 통계

적 분석을 하였다. Receiver operating characteristic(ROC)를 이용하여 관류지도의 유용성에 대한 평가를 하였다.

결과: 각 픽셀의 시간-농도 함수를 이용하여 Volume map, Washout map, Peak map, 그리고 TTP map 을 구성하였고, 이 관류지도를 통해 공동성 종괴의 관류정도가 표현되었다. 총 23례의 화농성 공동성 종괴 중, 16례(69.6%)에서 약한 washout 과 느려진 TTP를 보였다. 반대로 15례의 악성 공동성 종괴 중, 11례(73.3%)에서 뚜렷하게 강한 washout 을 보였다. 15례의 결핵성 공동성 종괴 중, 9례(66.7%) 에서 Volume map 과 Peak map에서 모두 낮은 정도의 관류를 보였다. 일치도는 통계학적으로 유의하게 높았고 ($p=0.002$, $p=0.001$, $p=0.001$, $p=0.001$), 모든 경우에서 고식적 CT보다 관류CT를 같이 이용한 경우에 높은 진단 능력을 보였다. (Az값 차이들은 각각 0.132, 0.163, 0.167이며, 유의수준은 각각 $p<0.040$, $p<0.020$, $p<0.042$ 이었다).

결론: 역동적 CT를 이용한 관류 영상은 공동성 종괴의 감별진단에 유용한 방법으로, 공동성 종괴의 비침습적 진단 및 적절한 치료계획 수립에 도움이 되는 유용한 진단도구이다.

핵심되는 말: 공동, 폐, 흉부, 관류 CT, CT